

MICROSTRUCTURE OF TITANIUM WELDS

Paul Danielson, Rick Wilson, and David Alman
U. S. Department of Energy, Albany Research Center

Introduction

An intimate knowledge of the processing-microstructure-property relationships is paramount in solving difficult materials problems. Whether the problem is related to failure analysis, materials substitution, or materials development, microstructural analysis is a key activity required to formulate a solution. To demonstrate the strength and flexibility of microstructural analysis we examined two weld joints in commercial purity titanium (CP-Ti). During Gas Tungsten Arc Welding (GTAW), one joint was protected from the environment. The other joint was deliberately not protected, and thus, was contaminated with impurities.

The microstructure of titanium and titanium alloys can be very complex, because titanium undergoes an allotropic phase transformation at 882°C (alpha (HCP) → beta (BCC)). This is similar to the well-known ferrite to austenite transformation in iron and steels. Thus, depending on processing, the microstructure of titanium can vary widely. For instance, annealed titanium can consist of an equilibrium microstructure with equiaxed grains, whereas, titanium that has been rapidly cooled can form metastable phases, such as martensite or bainite, and possess Widmanstätten plates or have an acicular microstructure.

During welding, a small portion of the titanium is melted and rapidly cooled. The complexities of the resultant microstructure can be compounded by contamination with impurities from the ambient environment (i.e., O₂, N₂). In small amounts, these elements do not change the HCP crystal structure; but because these elements are small they locate on interstitial sites in the crystal lattice and prevent the movement of dislocations, thereby significantly increasing the hardness and strength, thus causing embrittlement of the weld joint. Further, Ti readily oxidizes when heated in an air environment. Therefore, whenever titanium is welded, a protective inert covering gas like argon or helium must be used to prevent microstructural degradation.

The properties (high specific strength, modulus, corrosion resistance, etc.) of titanium make it attractive for many applications. There are numerous applications where developing reliable and economical joining procedures may be a limiting factor in utilizing Titanium's unique properties. Thus, it is important to understand the influence of joining variables on the properties of titanium welds.

Titanium plate welding process:

For this study, 6.35 mm (0.25 in) CP-Ti plates were joined. A bulk chemical analysis of the plate is listed on Table I. The region of the CP-Ti plate to be joined was cut and machined to a 60° bevel angle. The joint was cleaned with a new stainless steel brush to remove any oxides or metallic debris and rinsed with clean acetone to remove any oil from the machining process. Immediately after cleaning, the plates were welded to minimize contamination.

Joining was accomplished by GTAW and CP-filler wire in four passes. Argon was used as the inert covering gas. CP Ti filler wire (4.8 mm (0.19 in) diameter) was used in all the welds with straight polarity DC current. The chemical composition of the filler is also listed in Table I. To examine the influence of contamination on the microstructure, one set of plates was welded with the first two passes inside an argon filled glove box, and two subsequent passes outside the glove box with argon covering gas from the GTAW torch. The second set was welded entirely outside the glove box with four passes using only the argon covering gas for protection.

Metallographic sample preparation:

Prior to metallographic examination of the welds, the mechanical properties of the welds were determined by three-point-bend testing of the joined plates. Bend specimens were machine cut from the welded plate. The dimensions of the specimens were approximately 75 mm long by 25 mm wide by the thickness of the plate (6.35 mm). The span length of the 3 pt. bend jig was 50 mm long. The top of the weld was oriented towards the tensile side of the 3 pt. bend configuration. Testing was done on a screw driven universal testing machine with a constant crosshead speed of 5 mm per minute.

The welded samples were prepared for optical bright field reflected light microscopy and Scanning Electron Microscopy. First, 19.05 mm (0.75 in) square samples were cut with the hack saw from the welded coupons used as bend specimens and mounted in thermoset polymeric mount material. (Note: microstructural examination was performed on welds that had been mechanically tested in 3-pt. bending.) The mounted specimens were ground and polished to a 0.25 μm finish. Etching procedures were used to expose the underlying microstructural features including grain boundaries, inclusions, cracks, and secondary phases. Solutions that can be used for etching titanium include: 100 ml water, 2 ml HF, 5 ml HNO_3 (Krolls Etch); or 20 ml water, 10 ml 40% KOH, 5ml 30% H_2O_2 ; or 30 ml glycerin, 10 ml Hf, 10 ml HNO_3 . The polished metallographic mount can be immersed or swab etched in the solution from 3 to 10 seconds to reveal the microstructural features.

Characteristics of Titanium Welds as Revealed from Metallographic Examination:

Table I compares properties of the welds with those of the base metal. Both welds were not as strong as the base plate. The strength of the low oxygen weld was about 67% that of the base plate, while the strength of the high oxygen weld was only 25% of the starting plate. The analyzed bulk oxygen content of the low oxygen weld is essentially the same as the base plate and the filler wire; however, the analyzed bulk oxygen content is more than twice in the high oxygen weld compared with the base plate and the filler wire. Metallographic analysis was used to correlate the mechanical response and bulk chemical analysis of with the microstructures of the joints.

The Low Oxygen Weld:

Low magnification cross sections of this weld are illustrated in Figures 1 and 2. The unetched view (Fig. 1a) shows the cracks from the bend testing, as well as Vickers micro-hardness indentations placed down the weld centerline (from the top to the bottom) and across the weld (from the centerline through the heat-affected-zone (HAZ) and into the base metal). The etched microstructure (Fig. 1b) reveals the grain structure in the weld. The various colors were formed due to differences in thickness of the oxide film formed during the preparation of metallographic specimens. The microstructure at the midpoint of the weld centerline (Figure 2) consists of a typical alpha titanium microstructure. The low temperature, HCP, alpha phase cells are small (10 μm) and high temperature, BCC, beta phase decorate the grain boundaries. The grain size at weld centerline is 1 mm. Figure 3 shows a high magnification micrograph of the transition between the HAZ and the base metal. Across the weld the grain size decreases from 1 mm (1000 μm) at the centerline to 20 μm at base metal. In the base metal the alpha phase grains are equiaxial in shape and are oriented in the rolling direction. In the center of the plate the grains are elongated due to rolling. The light colored spots at the periphery and inside some of the alpha phase grains as shown in Figure 4 are reinvents of the high temperature beta phase grain boundaries within.

The Vickers hardness values are plotted in Figure 5 (down the weld centerline) and Figure 6 (across the weld), along with oxygen, nitrogen and carbon concentrations obtained adjacent to each indent using SEM coupled with Energy Dispersive X-ray (EDX) analysis. Due to the nature of the EDX analysis, these values can only be used for comparative purposes, and are not actual values. The oxygen content and hardness increased towards the top of the weld (Fig. 5). The values for the carbon and nitrogen remained relatively constant. These results suggest that the increase in hardness is directly related to the oxygen concentration along the weld centerline. Across the weld, the hardness was lower at the centerline, increased in the heat-affected zone, and decreased to a constant value in the base metal (Fig. 6). The oxygen, nitrogen and carbon contents were essentially constant across the weld.

Several interesting features were observed at the surface of the weld (Fig. 7 and 8). These include cracks from the bend test, low temperature alpha cells, large beta grain boundaries, twins and an oxide surface layer that contains micro-cracks (Fig. 7). The origin of the micro-cracks is potentially due to the strains associated with thermal expansion mismatch that developed in the brittle titanium oxide layer during rapid cooling. A higher magnification view of the surface (Fig. 8) reveals small holes or voids just below the oxide surface layer. SEM analyses revealed these holes were uniform in size, spacing, shape and depth from the surface and aligned perpendicular to the bending direction (Fig. 9). The source of the holes was not obvious, and they may have resulted from: (i) solidification defect; (ii) entrapped covering gas or oxygen; or (iii) an artifact from the bending test. Higher magnification views (Figure 10) revealed the surface of the voids as dimpled. A dendritic surface would have indicated the holes were formed during solidification due to shrinkage voids. A smooth surface would have developed from gas porosity. However, since the surface is dimpled, they were probably formed during bending. Figure 11 shows micrographs of the holes in which the specimen was prepared by polishing down from the surface of the weld. These micrographs also reveal that the holes form perpendicular to the bending direction and that the surface is dimpled. The micrographs in Figures 10 and 11 are consistent

with a void coalescence failure mechanism observed in ductile materials when they are stressed beyond the yield point, and hence, they formed during the bend testing.

The High oxygen Weld:

Low magnification cross sections of a high oxygen titanium weld are shown in Figure 12. These cross sections show the cracks from the bend test and Vickers microhardness indentations placed in various locations in the weld. Similar to the low oxygen weld, the microstructure at the midpoint of the weld centerline (Figure 13) consists of a typical alpha titanium microstructure with small alpha phase (10 μm) cells and beta phase decorating the grain boundaries.

Deformation twins can also be seen in the upper right hand corner of the optical photomicrograph. Illustrated in Figure 14 is a higher magnification of the weld, HAZ, and the base metal with the micro-hardness indents. Again, similar to the low oxygen weld, the grain size at weld centerline is 1 mm and from the weld centerline to the base metal the grain size decreases from 1mm to 20 μm .

The Vickers hardnesses and impurity concentrations (determined by EDX) adjacent to each indent are plotted in Figures 15 (down the weld center line) and 16 (across the weld). Similar to the low oxygen weld, the hardness and oxygen content increase toward the weld surface.

Significant oxygen contamination is observed at the top of the weld metal pass as illustrated in Figure 17 by the yellow color changes in the microstructure. An acicular microstructure with Widmanstätten plates and beta phase along grain boundaries are visible. At higher magnifications (Figure 18), an alpha phase basket weave microstructure and retained dark remnants of metastable beta phase between the alpha cells are also visible. The coring formed in the alpha cells is a result of the peritectic phase reaction that occurs between Ti and TiO_2 at 1740°C (see reference 4). During the rapid cooling associated with welding, oxygen helps retain a portion of the high temperature beta phase in the microstructure at room temperature.

Comparison of the Welds

Similar microstructures developed in the interior of the welds and HAZ in the two joints. It is not surprising that the low and high oxygen welds have similar grain sizes. Since the heat input during welding of both joints was the same, it is expected that joints with similar grain sizes should develop. The difference in microstructure occurs at the weld surface. Significant oxygen contamination caused the surface of the high oxygen weld to comprise an acicular microstructure with retained beta phase between alpha cells, Widmanstätten plates, and beta phase along grain boundaries. The surface of the low oxygen weld consisted of low temperature alpha cells and large beta grain boundaries. The hardness of the welds was not identical. Inspecting the values shown in Figures 5-6 and 15-16 reveal that the high oxygen weld is significantly harder than the low oxygen weld. This is expected as the oxygen will embrittle Ti, and is manifested in the significantly lower strength measured in the high oxygen weld.

References

1. Light Alloys sec. ed., Polmear, Edward Arnold, 1989.
2. Revealing Microstructures in Metals, R.L. Anderson, Scientific paper 425-C0000-P2, Westinghouse Research Laboratories, 1962.
3. The Principles of Metallographic Laboratory Practice, G.L. Kehl, McGraw-Hill, 1949.
4. Phase Diagrams for Ceramists, Levin, McMurdie and Hall, American Ceramic Society, P. 56, 1956.
5. Metallography of Titanium Alloys, H.R. Ogden and F.C. Holden, TML Report No. 103, Titanium Metallurgical Laboratory, Battelle Memorial Institute, 29 May 1958.

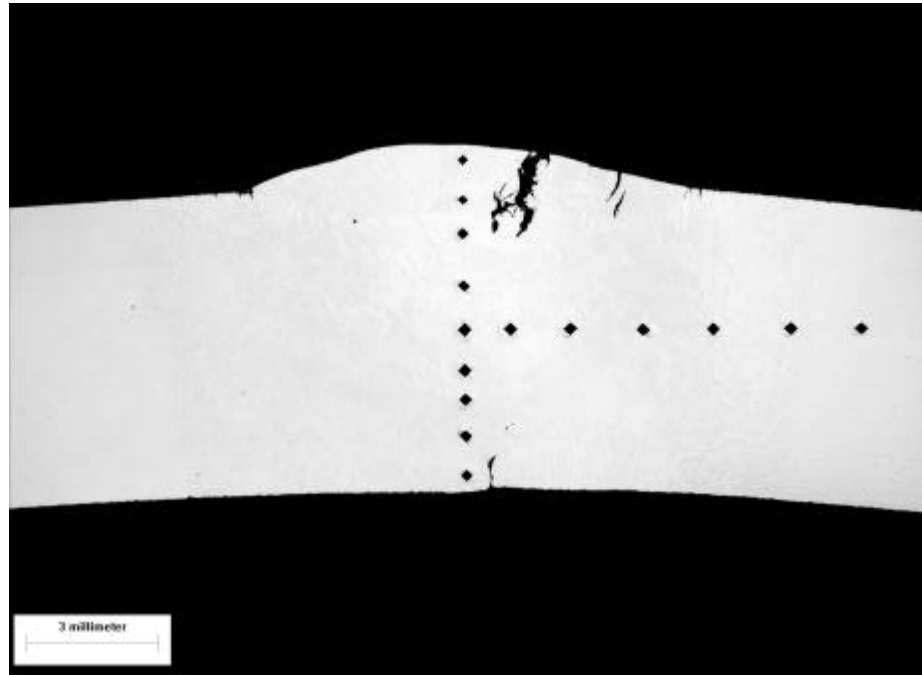
Table I. Properties of Titanium Materials and Welds

		CP-Ti Filler Rod	CP-Ti Plate	Low Oxygen Weld	High Oxygen Weld
Impurity Content (Wt%) by Bulk Chemical Analysis	O ₂	0.189	0.189	0.190	0.437
	N ₂	0.011	0.007	0.050	0.392
	C	0.029	0.021	0.019	0.038
Bend Strength (MPa)		N/A	109	73.3	27.5

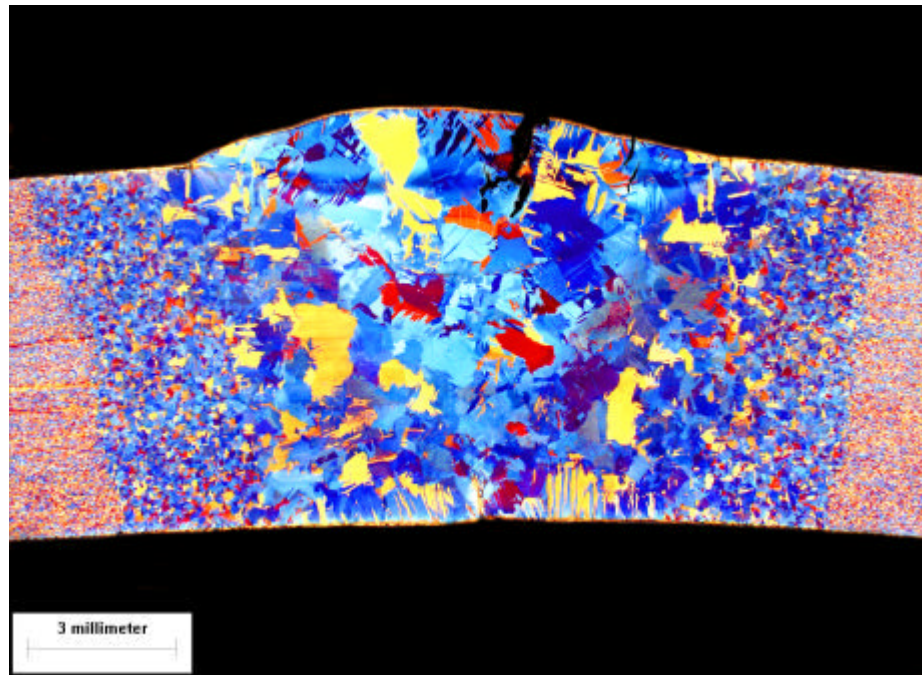
List of Figure Captions

- Figure 1. Cross-section low oxygen Ti weld: (a) unetched microstructure; (b) etched microstructure. Visible cracks are from subsequent bend testing and Vickers hardness indent.
- Figure 2. High magnification view at the centerline of the low oxygen weld, showing a typical alpha Ti microstructure. Arrows point to high temperature beta phase boundaries (substructure in alpha cells).
- Figure 3. High magnification view of the HAZ zone of the low oxygen weld.
- Figure 4. Microstructure of the base Ti plate, showing equiaxed grains. White color spots (some identified by arrows) are remnants of the beta phase grain boundaries.
- Figure 5. Vickers hardness and impurity content profiles down the centerline (from top (position 0 mm) to bottom) of the low oxygen weld.
- Figure 6. Vickers hardness and impurity content profiles from the center of the weld (distance 0 mm) into the base metal of the low oxygen weld shown.
- Figure 7. Surface of the low oxygen weld (after bend testing). Visible are: (a) alpha Ti cells; (b) beta Ti grain boundaries; (c) twins; and (d) surface oxide (TiO_2) layer.
- Figure 8. Periodic “holes” in/or near the surface layer of the low oxygen weld.
- Figure 9. SEM micrograph of the “holes” in or near the surface layer.
- Figure 10. Various high magnification SEM micrograph of the “holes” in or near the surface layer, showing the dimpled surface of the “holes”.
- Figure 11. Cross section of the “holes” in or near the surface, verifying that these features are perpendicular to the bending direction: (a) optical micrograph; (b) SEM micrograph.
- Figure 12. Cross-section high oxygen Ti weld: (a) unetched microstructure; (b) etched microstructure. Visible cracks are from subsequent bend testing and Vickers hardness indent.
- Figure 13. High magnification view at the centerline of the high oxygen weld, showing a typical alpha Ti microstructure. Arrow “a” points to high temperature beta phase boundaries; Arrow “b” points to deformation twins.
- Figure 14. View of the HAZ of the high oxygen weld.

- Figure 15. Vickers hardness and impurity content profiles down the centerline (from top (position 0 mm) to bottom) of the high oxygen weld.
- Figure 16. Vickers hardness and impurity content profiles from the center of the weld (distance 0 mm) into the base metal of the high oxygen.
- Figure 17. Microstructure of the high oxygen weld showing alpha phase basket weave (arrow "a") and remnants of beta phase between alpha cells (arrow "b").
- Figure 18. Higher magnification view of the near surface microstructure of the high oxygen weld showing coring of the alpha phase.
- .



(a)



(b)

Figure 1. Cross section low oxygen Ti weld: (a) unetched microstructure; (b) etched microstructure. Visible are cracks are from subsequent bend testing and Vickers hardness indent.

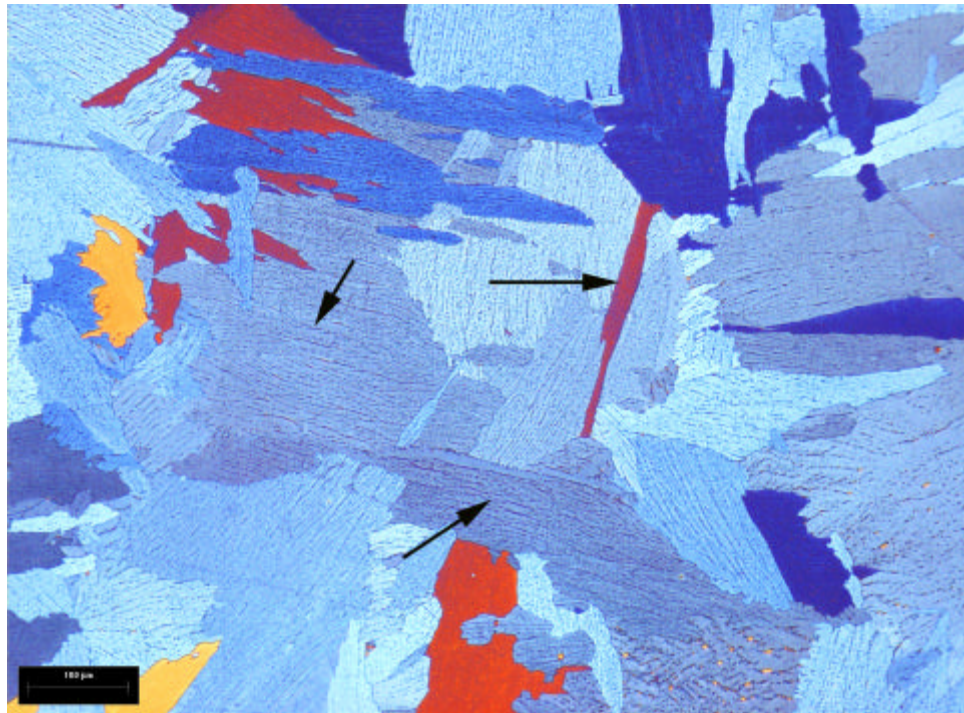


Figure 2. High magnification view at the centerline of the low oxygen weld, showing a typical alpha Ti microstructure. Arrows point to high temperature beta phase boundaries (substructure in alpha cells).

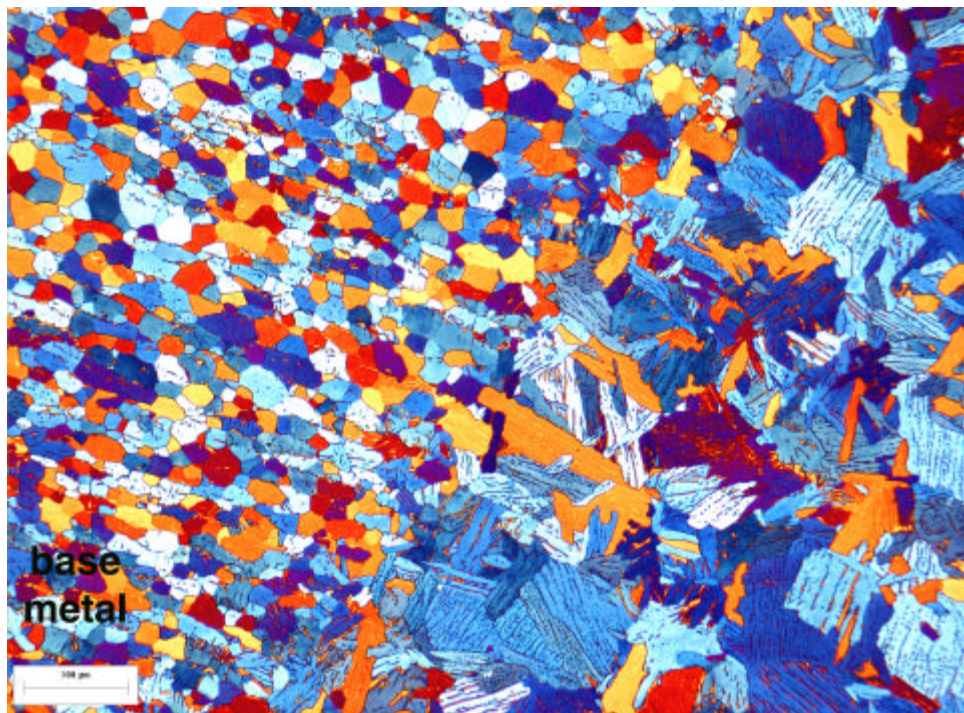


Figure 3. High magnification view of the HAZ of the low oxygen weld.

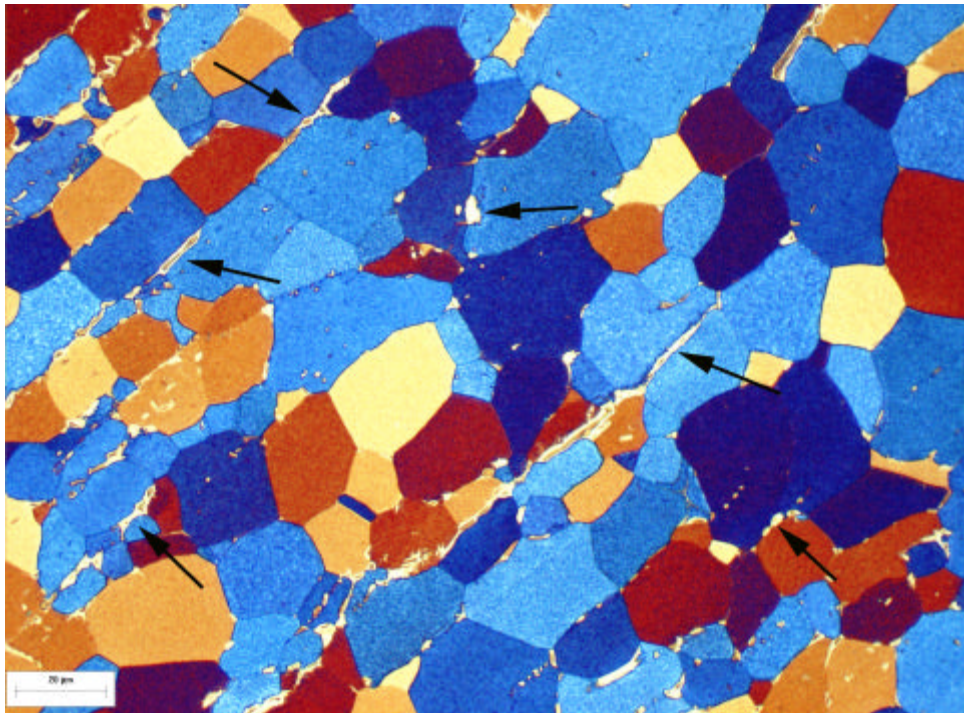


Figure 4. Microstructure of the base Ti plate, showing equiaxed grains. White color spots (some identified by arrows) are remnants of the beta phase grain boundaries.

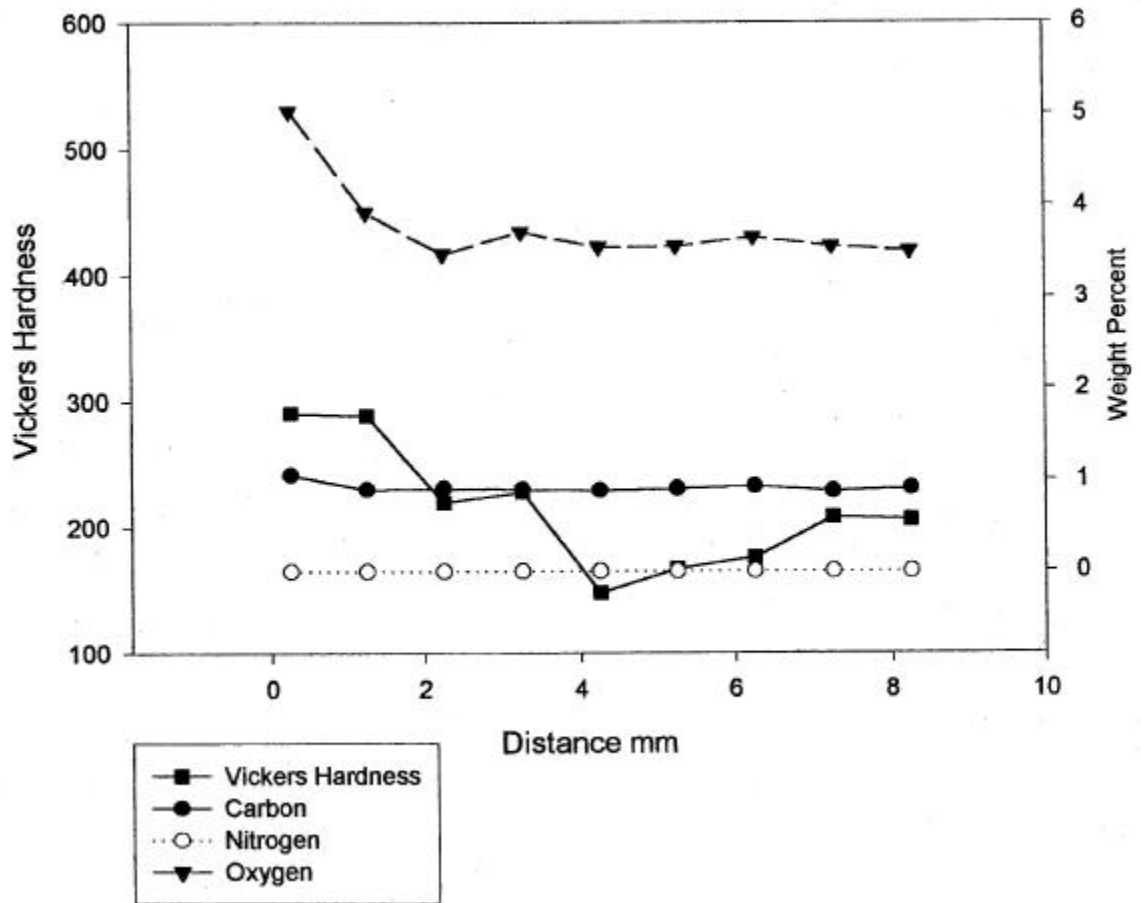


Figure 5. Vickers hardness and impurity content profiles down the centerline (from top (position 0 mm) to bottom) of the low oxygen weld.

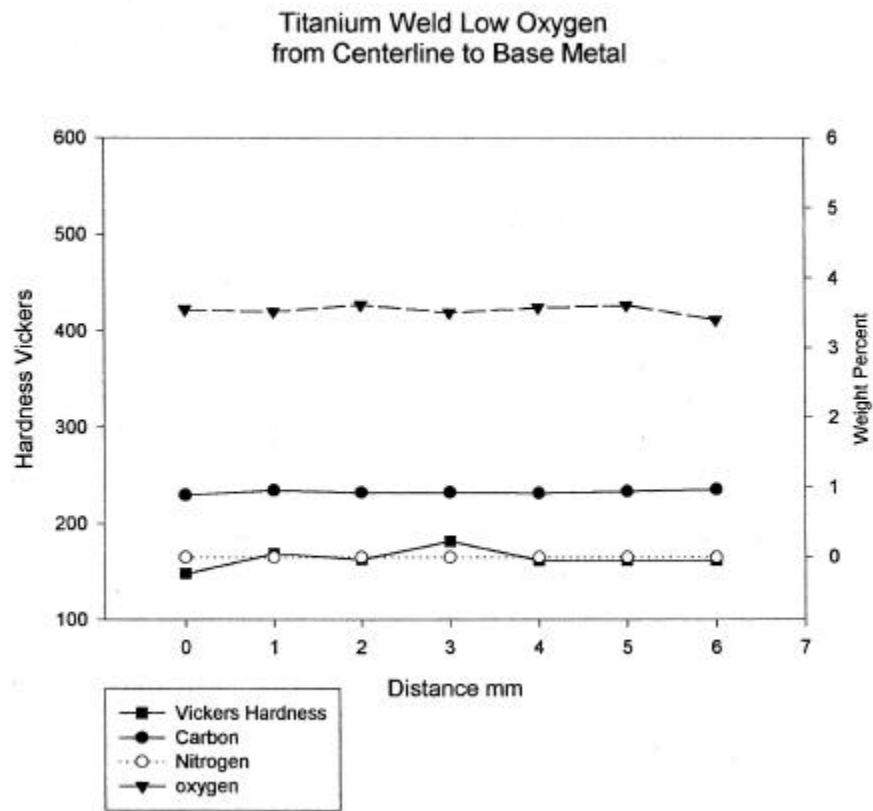


Figure 6. Vickers hardness and impurity content profiles from the center of the weld (distance 0 mm) into the base metal of the low oxygen weld shown.

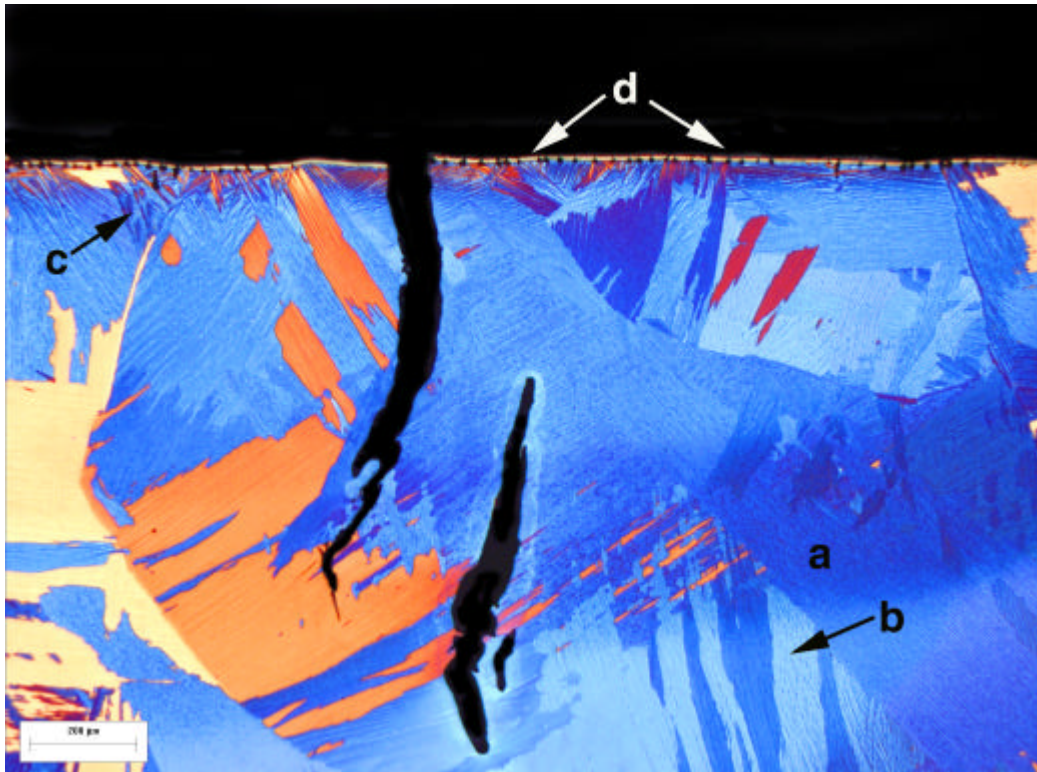


Figure 7. Surface of the low oxygen weld (after bend testing). Visible are: (a) alpha Ti cells; (b) beta Ti grain boundaries; (c) twins; and (d) surface oxide (TiO_2) layer.

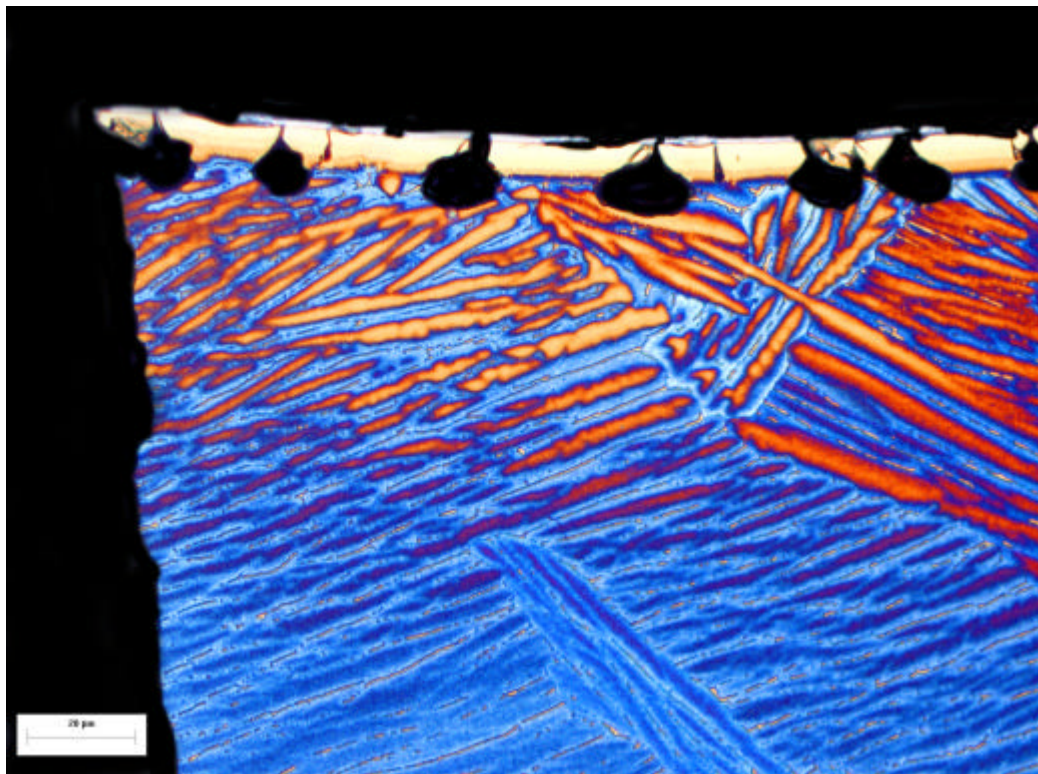


Figure 8. Periodic "holes" in or near the surface layer of the low oxygen weld.

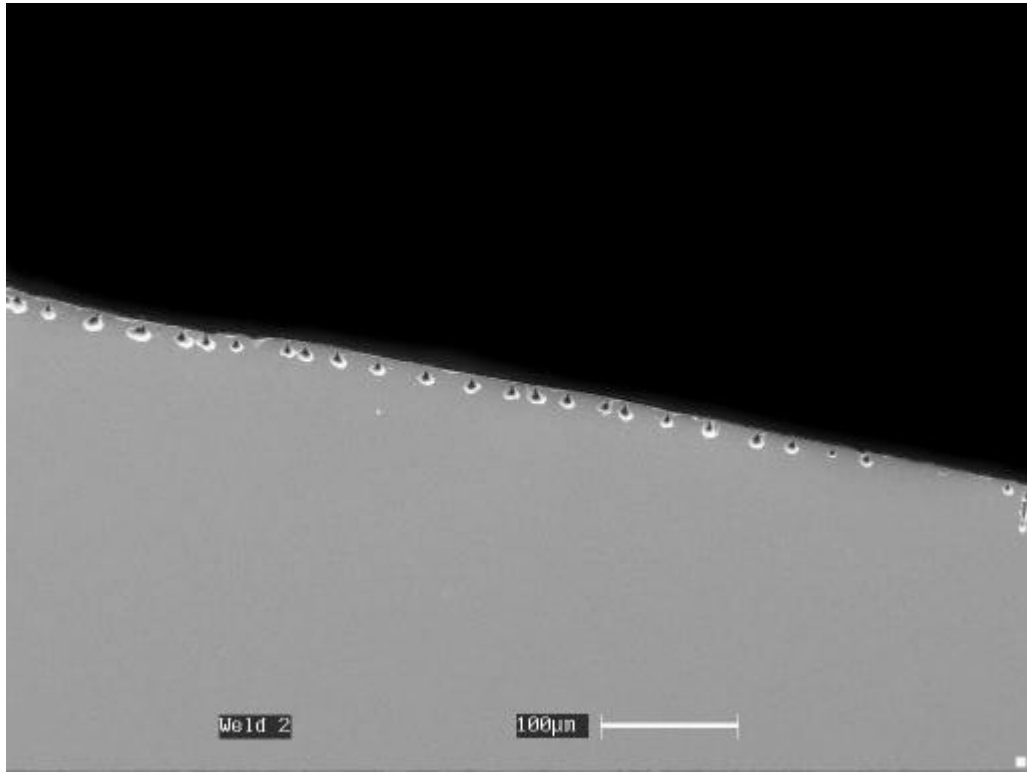
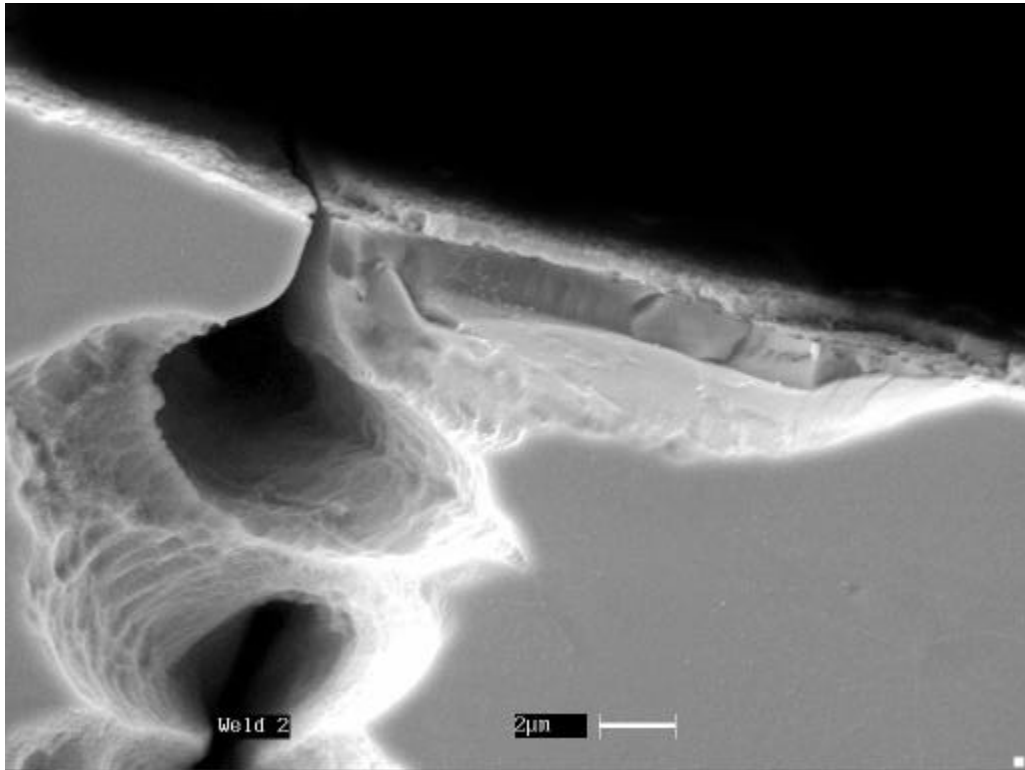
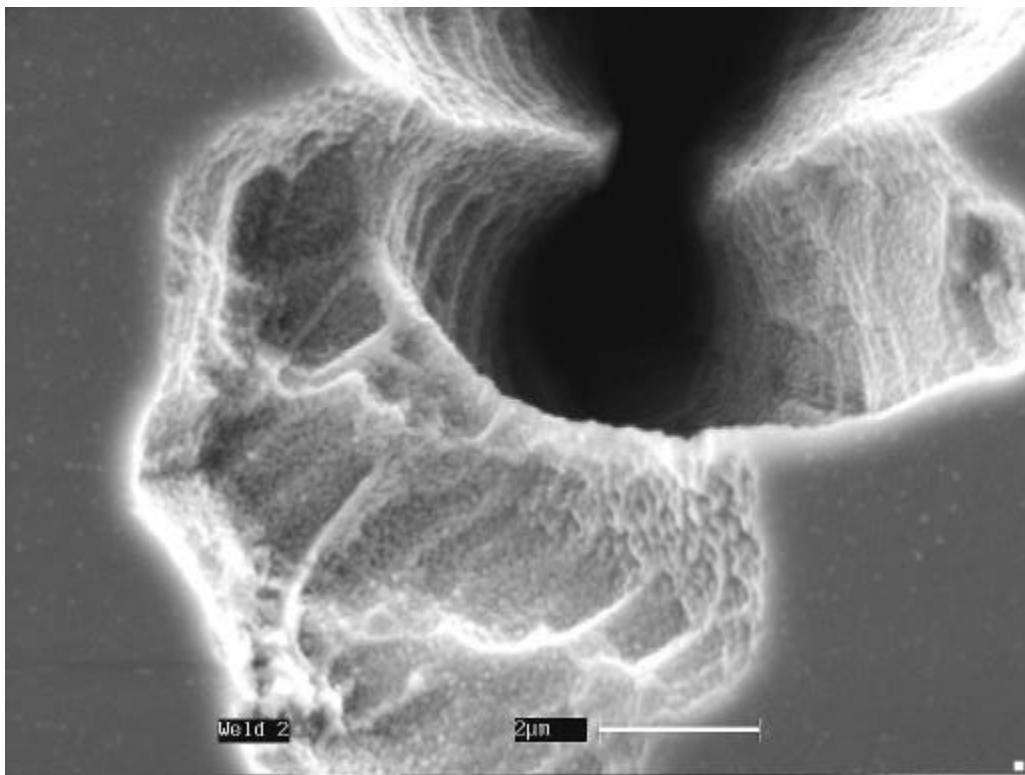


Figure 9. SEM micrograph of the “holes” in or near the surface layer.

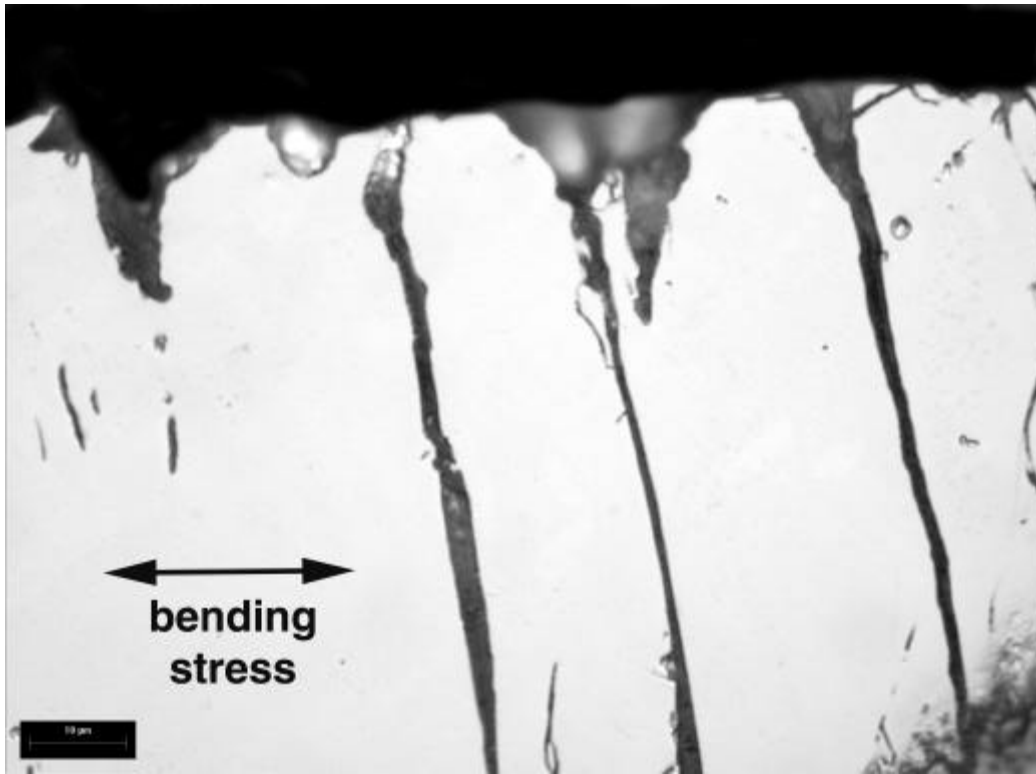


(a)

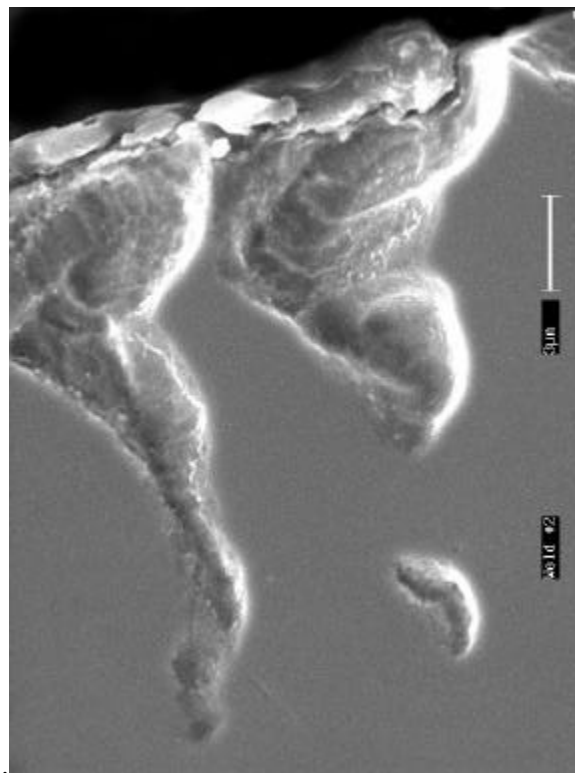


(b)

Figure 10. Various high magnification SEM micrograph of the “holes” in or near the surface layer, showing the dimpled surface of the “holes”.

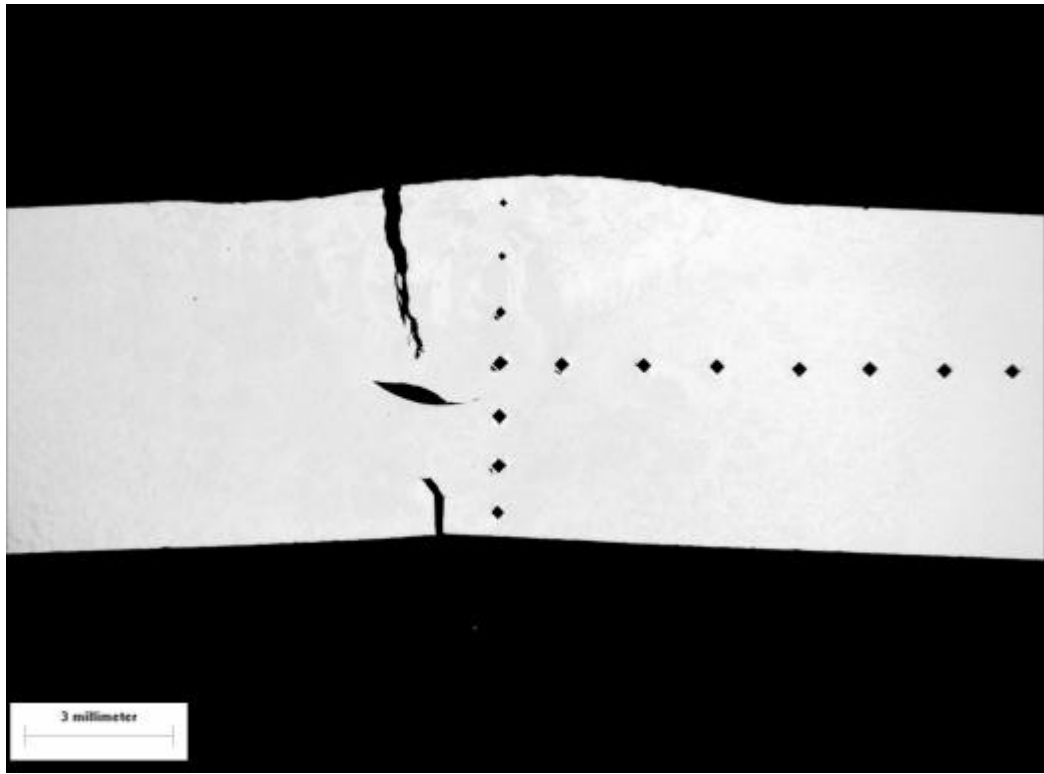


(a)

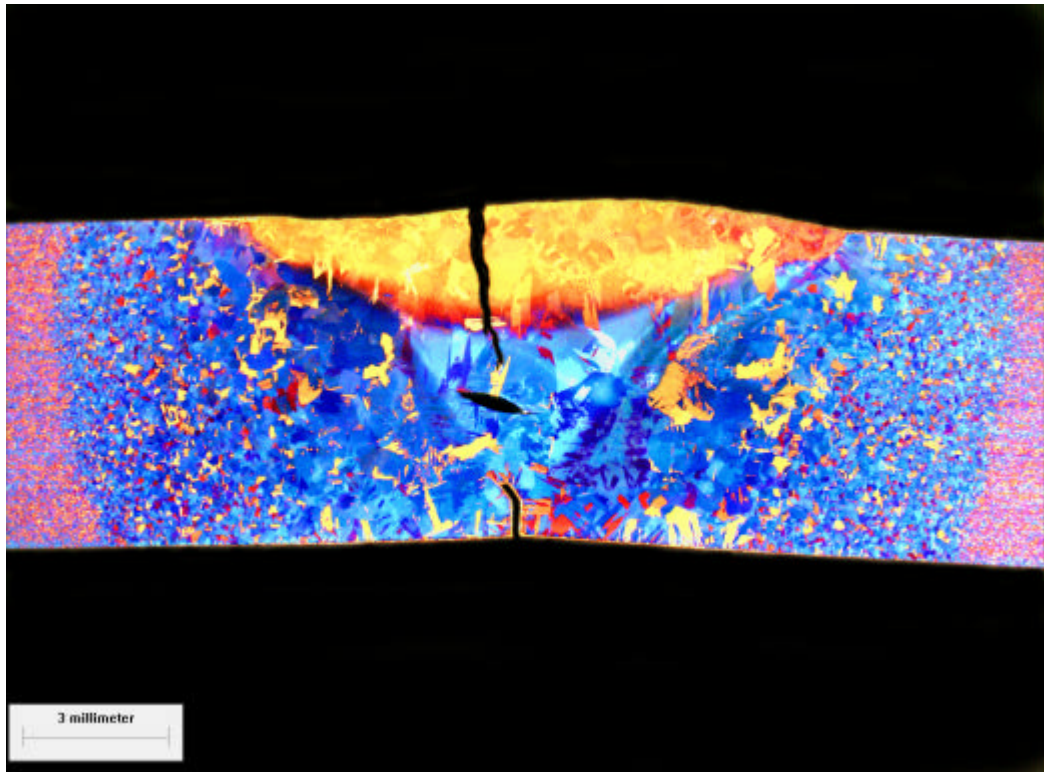


(b)

Figure 11. Cross section of the “holes” in or near the surface, verifying that these features are perpendicular to the bending direction: (a) optical micrograph, (b) SEM micrograph



(a)



(b)

Figure 12. Cross-section high oxygen Ti weld: (a) unetched microstructure; (b) etched microstructure. Visible are cracks are from subsequent bend testing and Vickers hardness indent.

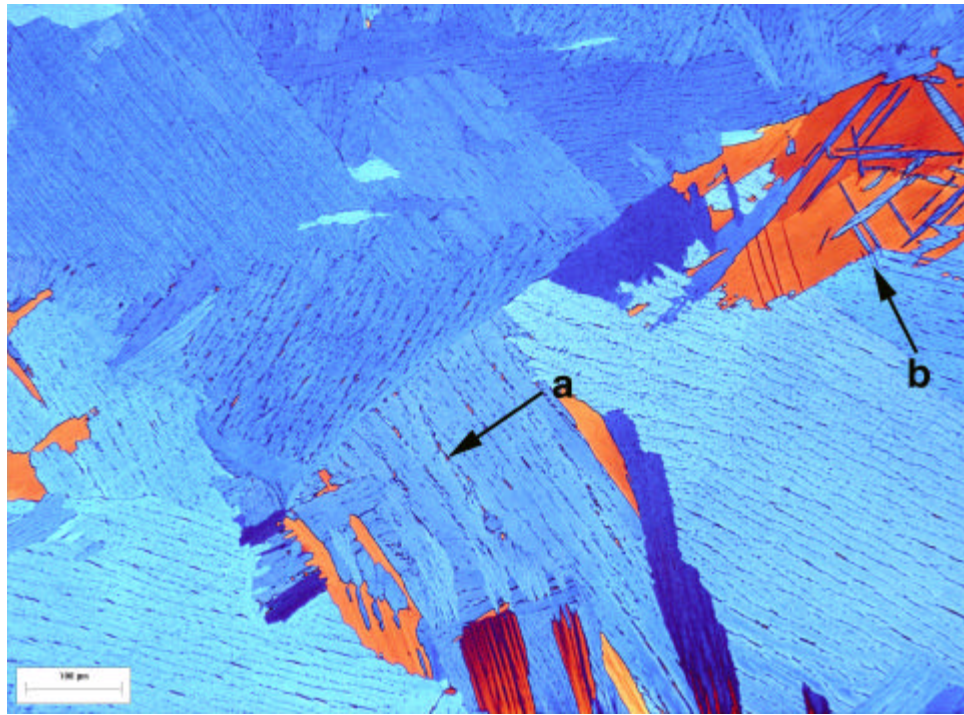


Figure 13. High magnification view at the centerline of the high oxygen weld, showing a typical alpha Ti microstructure. Arrow “a” points to high temperature beta phase boundaries; Arrow “b” points to deformation twins.

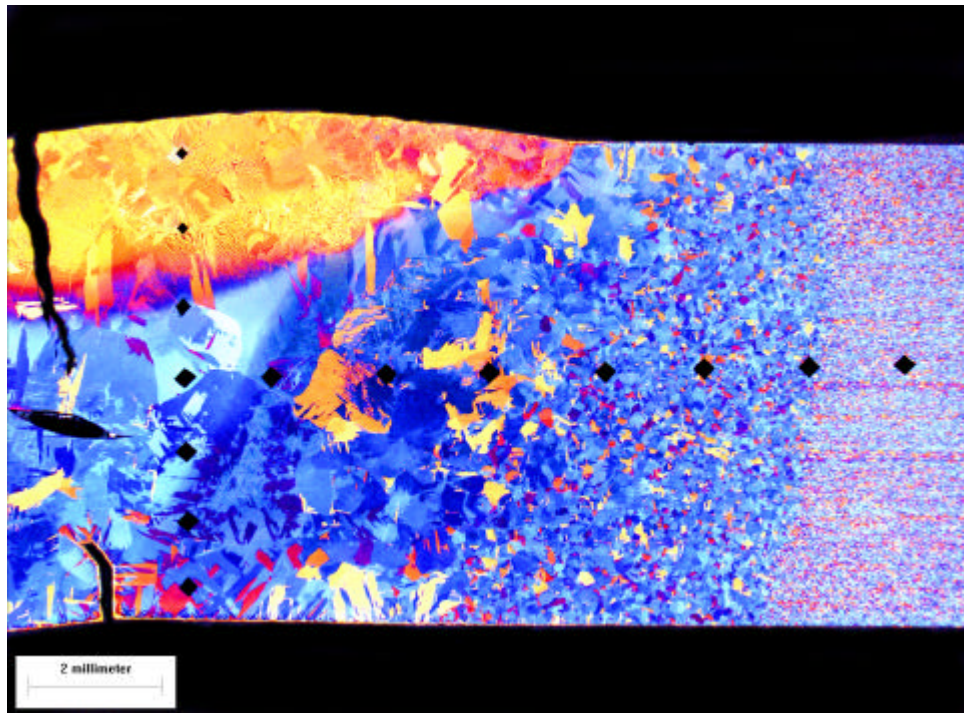


Figure 14. View of the HAZ of the high oxygen weld.

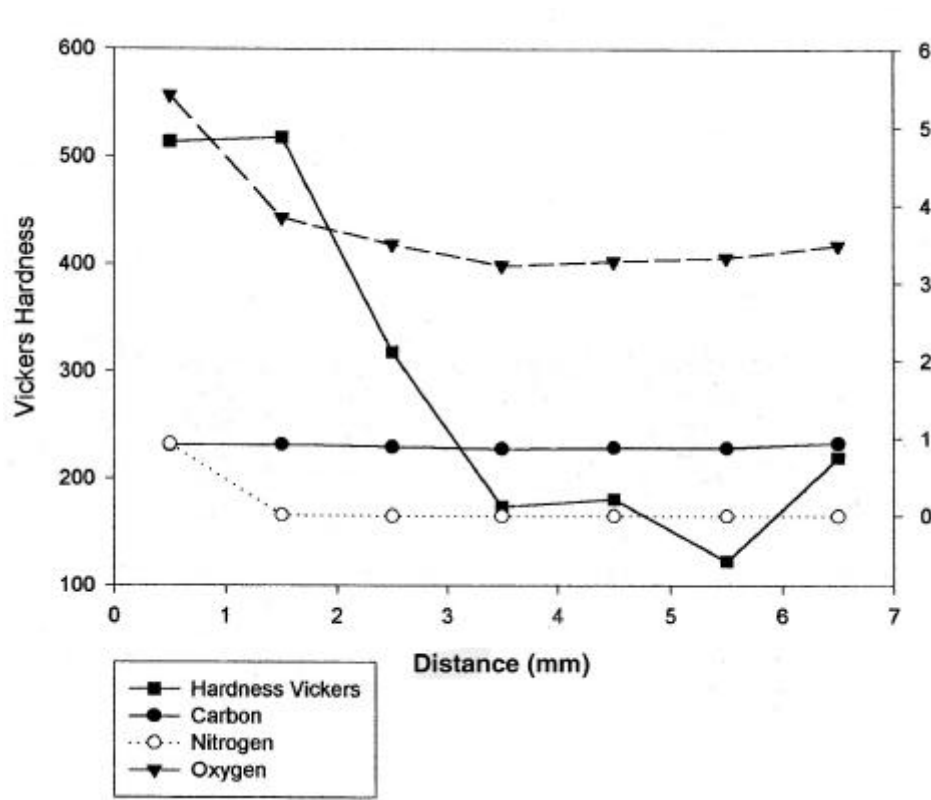


Figure 15. Vickers hardness and impurity content profiles down the centerline (from top (position 0 mm) to bottom) of the high oxygen weld.

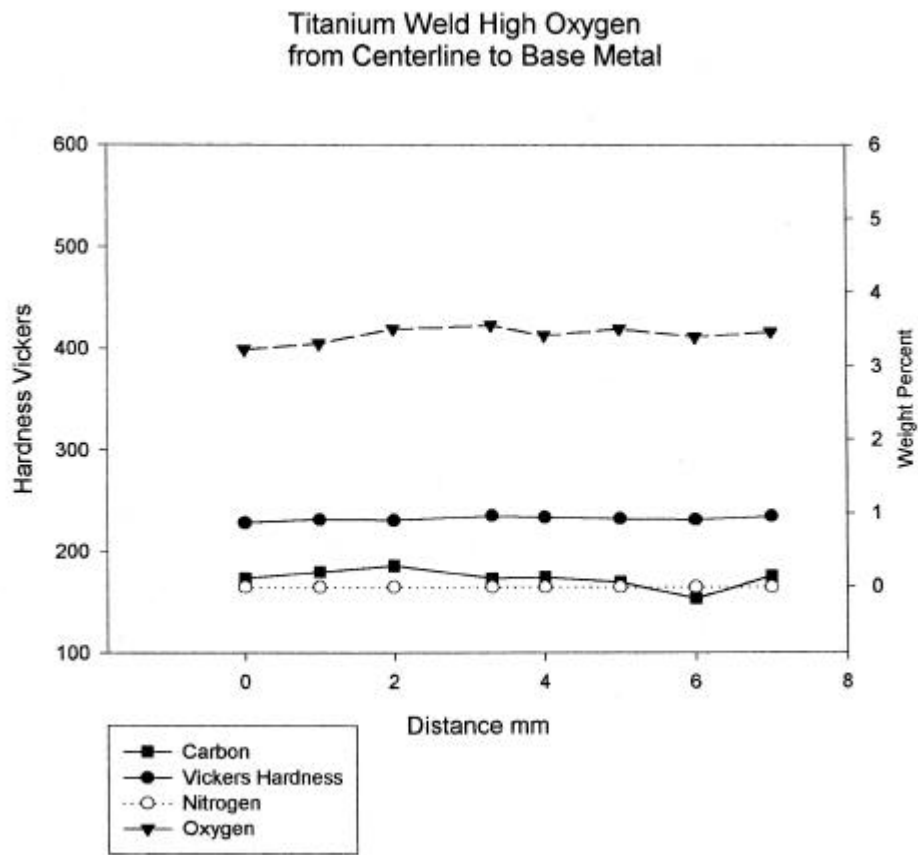


Figure 16. Vickers hardness and impurity content profiles from the center of the weld (distance 0 mm) into the base metal of the high oxygen.

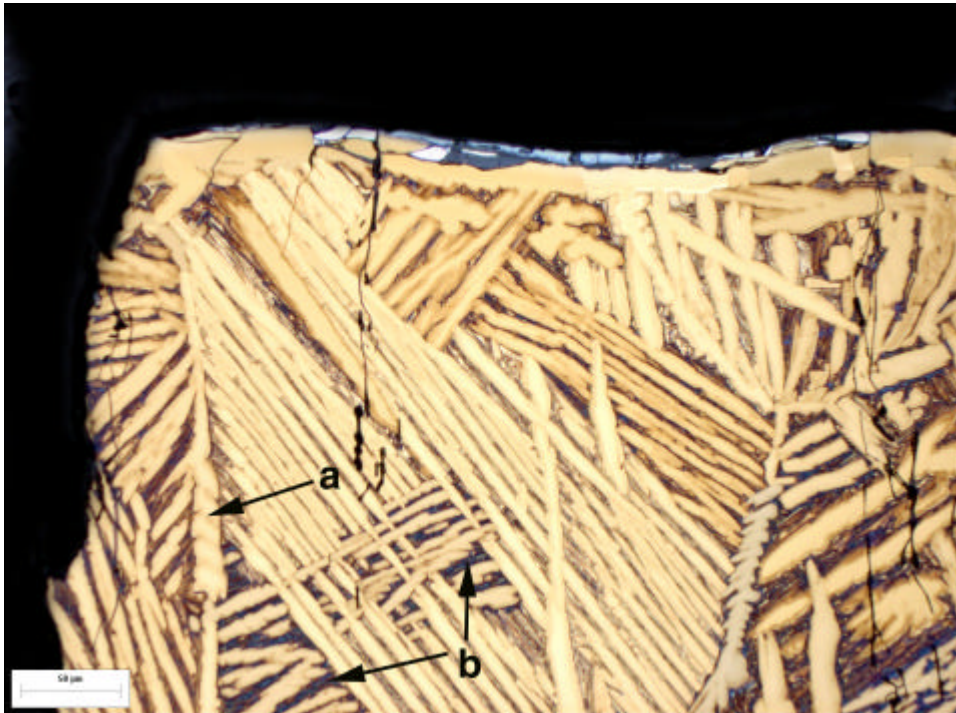


Figure 17. Microstructure of the high oxygen weld showing alpha phase basket weave (arrow “a”) and remnants of beta phase between alpha cells (arrow “b”).

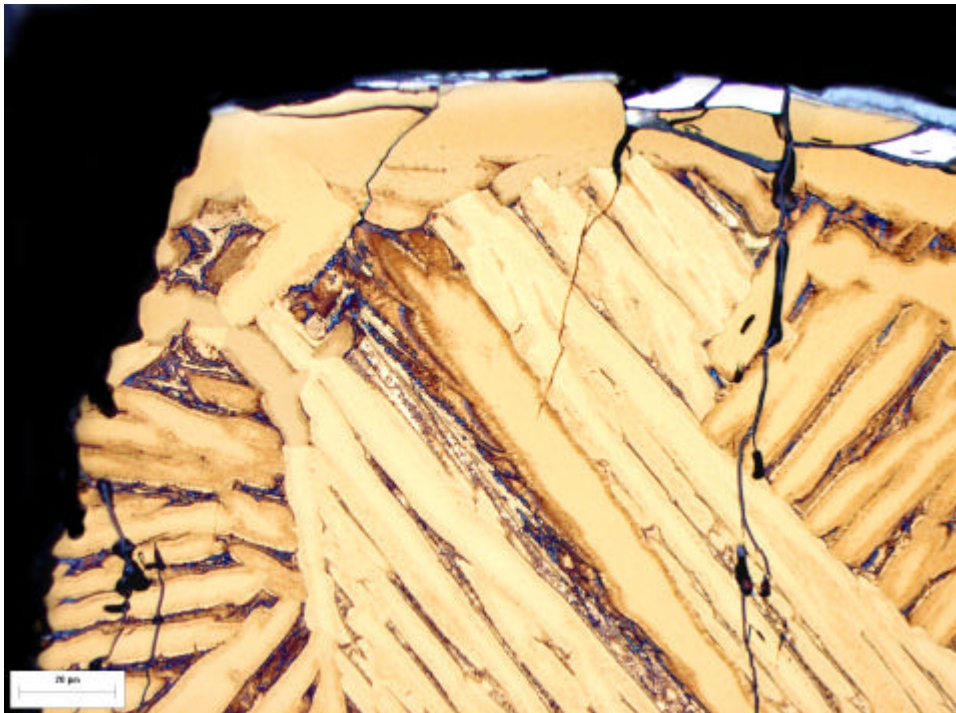


Figure 18. Higher magnification view of the near surface microstructure of the high oxygen weld showing coring of the alpha phase.